IEEE Access
Multidisciplinary | Rapid Review | Open Access Journal

Received April 20, 2022, accepted May 1, 2022, date of publication May 4, 2022, date of current version May 13, 2022.

Digital Object Identifier 10.1109/ACCESS.2022.3172711

Distributed Load Control Using Reliable Low-Data-Rate Power Line Communication

ADEDAYO O. ADERIBOLE[1], KEVIN J. KIRCHER[1], (Member, IEEE), STEVEN B. LEEB[1], (Fellow, IEEE), AND LESLIE K. NORFORD[2]

[1]Department of Electrical Engineering and Computer Science, Massachusetts Institute of Technology, Cambridge, MA 02139, USA
[2]Department of Architecture, Massachusetts Institute of Technology, Cambridge, MA 02139, USA

Corresponding author: Adedayo O. Aderibole (adedayo@mit.edu)

This work was supported in part by the Exelon Corporation, and in part by The Grainger Foundation.

ABSTRACT Many demand-response schemes fail because they inconvenience consumers or add unnecessary costs. When participating in a typical demand-response scheme, a consumer may be subjected to invasive control systems, communication systems, or data collection. These demand-response schemes can quickly lose their novelty and may annoy customers by curtailing availability of their appliances, such as electric water heaters or air conditioners. This paper demonstrates a self-organizing demand response scheme that uses power lines as a natural, ''free'' infrastructure for communication. The approach can shave peak demand substantially with no inconvenience to or attention from the user. Tailored signaling schemes and a custom application of low-data-rate power line communication (PLC) enable loads to reliably self-organize their demand. Field experiments with thermostatically-controlled loads in an actively occupied, 24-floor apartment building demonstrate the advantages of the low-data-rate PLC scheme for energy control.

INDEX TERMS Demand-side management, low-data-rate communication, media access control, network access protocol, power line communication, time division multiple access.

I. BACKGROUND

The operation of thermostatically-controlled loads (TCLs), electric vehicle (EV) chargers, and many other loads can be coordinated to avoid unfortunate and unnecessary load peaking [1]–[5]. For TCLs, for example, a group of environmental control units (ECUs) in an apartment building might serve several different living spaces. These HVAC or ECU systems generally do not operate continuously. They cycle on and off to control temperature. Uncoordinated, these loads operate with a ''greedy'' strategy for maintaining a comfortable indoor environment. They can and do overlap in operation to create unfortunate demands on the electrical infrastructure, especially transformers and distributed-generation resources. However, there is another way. Intelligent loads can self-organize to avoid operating at times that would create unfortunate and unnecessary demand peaks [6]. For instance, a group of TCLs might be perfectly capable of maintaining occupant comfort with at most sixty percent of the loads operating on a rotating basis [5]. The operation of these loads can be interleaved to minimize peak demands for the group of loads or building while maintaining occupant comfort and quality of service. A communication network that connects these loads could be used to exchange digital tokens on a rotating basis to ensure a cap on the maximum number of loads operating at any instant in time. A reliable but low-bandwidth and low-cost network is necessary to enable loads to ''self-organize'' so that demand peaks are minimized.

Demand-response control schemes for ''slow'' loads do not require high data rates and can tolerate relatively long communication times. That is, the time-constants of the systems under control are sufficiently long to permit relaxed communication bandwidth requirements. Regulated EV charging proposed in [7], coordination of TCLs proposed in [5] and [8], and daily automated meter readings (AMRs) aggregation are typical examples.

Power line communication (PLC) is very attractive as smart grid communication infrastructure [9]–[11], and especially so for self-organized loads. Self-organizing loads do not need to share identifying information, so privacy is maintained. The power line provides a natural ''bus'' structure, permitting a load to broadcast to all of its local neighbors in a single burst of communication. No information needs

The associate editor coordinating the review of this manuscript and approving it for publication was Giambattista Gruosso.

This work is licensed under a Creative Commons Attribution 4.0 License. For more information, see https://creativecommons.org/licenses/by/4.0/

be uploaded to an internet, and the proposed load control scheme requires no client-server services with an outside party. Security may be easier to maintain on a communication system that requires physical access (as opposed to wireless or internet access) to participate.

Reference [12] provides a detailed summary of many existing PLC network access or media access control (MAC) protocols. PLC MAC protocols are usually classified as either contention-free or contention-based. Contention-free protocols negate the possibility of messages colliding during transmission by advance coordination. They are typically employed in applications with predictable round-trip times and require accurate synchronization of devices [12]. Two common contention-free methods are time division multiple access (TDMA) [13]–[16] and polling [17], [18]. Contention-based protocols such as carrier sense multiple access/collision avoidance (CSMA/CA) allow multiple users to access the network without prior coordination [19]–[21]. They do not require synchronization, but collisions increase with network size, leading to higher access delays and starvation for lower priority devices.

Although power lines are widely deployed for smart grid communication [9]–[11], they experience high signal attenuation due to multipath fading and circuit loading [22]. A common technique for ameliorating, but not eliminating, these problems deploys robust spread-spectrum techniques at data rates of 500 kilo bits-per-second (kbps) or less in the defined narrowband PLC (NB-PLC) frequency range (3-500kHz) [23]. In recent work, the authors showed that when much lower data rates are adequate, additional reliability in the NB-PLC range can be achieved by taking advantage of quasi-peak (QP) regulations governing PLC in certain frequency bands [3]. For example, low-data-rate applications that require less than 20-bps data rates benefit from the QP regulations by employing chirp spread-spectrum-QP-PLC (CSS-QP-PLC) signaling. This paper further enhances the performance of CSS-QP-PLC and demonstrates that a time division multiple access (TDMA) CSS-QP-PLC protocol can serve low-data-rate demand-response applications while avoiding network collisions and unpredictable access delays. Also in this paper, a series of challenging field experiments demonstrate the usefulness of the novel PLC approach described above for effective and non-intrusive load control.

Section II proposes a distributed repeating scheme to further enhance the performance of low-data-rate PLC. This scheme extends the functionality of CSS-QP-PLC signaling to allow modems, distributed within a PLC system, to act as repeaters based on the QP regulations framework. Section III presents a contention-free network access protocol based on TDMA to preserve the low-data-rate property of CSS-QP-PLC signaling while enabling maximum transmitted power per bit. Existing TDMA-based protocols do not exploit these modifications possible with low data rates, and therefore cannot leverage the QP regulations to improve low-data-rate PLC reliability. The proposed access protocol also seamlessly integrates the distributed repeating scheme and automatically assigns TDMA slots to new loads. Practical issues affecting the implementation of the proposed network access protocol are presented in Section IV. Finally, Section V presents hardware and demonstrates the performance of the proposed network access protocol in a case study of distributed demand-leveling control for TCLs. Field experiments carried out in a 24-floor high-rise apartment building with difficult attenuation challenges demonstrate the efficacy of the proposed low-data-rate PLC system.

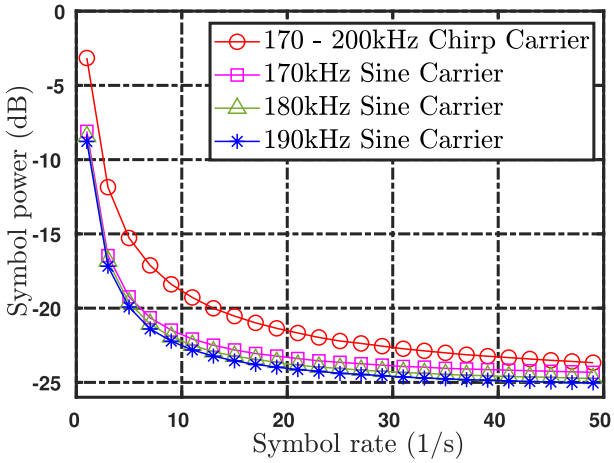

FIGURE 1. Impact of symbol rate on maximum transmitted power of various carrier signals based on the existing QP regulations [3].

II. PHYSICAL LAYER

In the proposed low-data-rate PLC network access protocol, the physical (PHY) layer leverages the QP conducted emissions limits by employing chirp signals to improve reliability and coverage [3]. This section restates one of the key results published in [3] to emphasize the merit of CSS-QP-PLC for low-data-rate applications. Afterwards, Section II-B presents the proposed distributed repeating scheme which further enhances the reliability of CSS-QP-PLC.

A. CSS-QP-PLC

Reference [3] provided the theoretical framework for CSS-QP-PLC, and demonstrated its ability to enhance the reliability of low-data-rate applications. For demand-response applications which do not require high data throughput, the QP conducted emissions limits in the 150-500-kHz frequency band permit carrier signals with low symbol rates to transmit more power per symbol. This is because the QP measurement procedure allows low-symbol-rate carrier signals to generate lower QP values than high-symbol-rate signals with equal amplitudes [3], [24], [25]. Therefore, within the governing rules, low-symbol-rate signals can be employed to transmit more power per symbol than high-symbol-rate signals. Fig. 1 demonstrates this phenomenon. For different carrier types leveraging the QP conducted

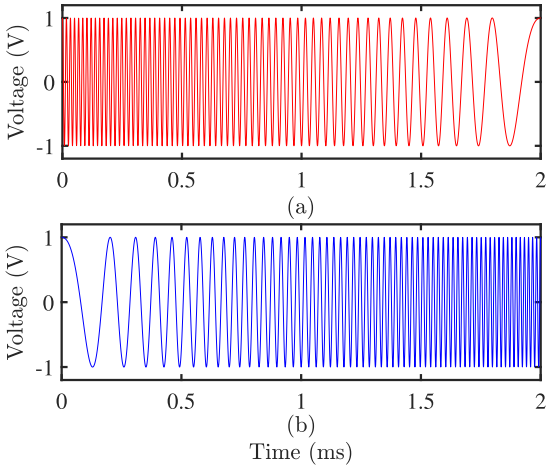

FIGURE 2. Illustration of chirp signals used to modulate data in the physical layer of the proposed low-data-rate PLC system. (a) "down-chirp" signal. (b) "up-chirp" signal.

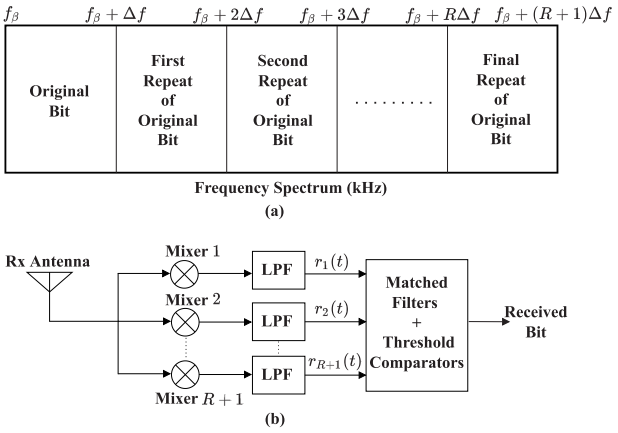

FIGURE 3. (a) Frequency-spectrum division in the proposed low-data-rate CSS-QP-PLC repeating scheme. (b) Low-data-rate PLC receiver bit decoding strategy with repeating.

emissions limits, the maximum allowable transmitted power per symbol increases as symbol rate decreases. Additionally, Fig. 1 also shows that chirp carriers can transmit more power per symbol than single-frequency carriers. This is because signals with wide bandwidths, like chirp signals, effectively leverage the QP conducted emissions measurement setup to operate at higher signal power [3] and [24]. A more in-depth analysis of the CSS-QP-PLC signaling scheme can be found in [3].

Due to the chirp signals' ability to operate at relatively higher signal power, the proposed low-data-rate network access protocol employs chirp signals to modulate data symbols. Fig. 2 provides an illustration of chirp signals used in this work. However, the methods presented in Section III also apply to other carrier signals. In this paper, a "down-chirp" shown in Fig. 2(a) and represented by

$$x_0(t) = A_0(t)\cos[2\pi f_0 t - \pi|\mu|t^2 + \theta_0] \tag{1}$$

modulates a "0" symbol, while an "up-chirp" shown in Fig. 2(b) and given by

$$x_1(t) = A_1(t)\cos[2\pi f_1 t + \pi|\mu|t^2 + \theta_1] \tag{2}$$

modulates a "1" symbol. The amplitudes of the carriers are denoted by $A_0(t)$ and $A_1(t)$, f_0 and f_1 are the initial frequencies, $|\mu|$ is the chirp rate, while θ_0 and θ_1 are the phases at time, $t = 0$. For example, the initial frequencies of the chirp signals shown in Fig. 2(a) and (b) are 180 kHz and 150 kHz, respectively. For both chirp signals shown in Fig. 2, the initial phases can be assumed to be zero and $|\mu|$ is $15 \times 10^6\ 1/s^2$.

Fig. 1 and other results published in [3] demonstrate the undeniable benefit of CSS-QP-PLC for low-data-rate applications. Consequently, the next part of this section proposes a repeating scheme that further enhances the reliability of low-data-rate PLC systems within the framework of the existing QP regulations.

B. PROPOSED REPEATING SCHEME

This section carefully tailors a repeating scheme to the existing QP regulations, further enhancing low-data-rate PLC reliability. A traditional repeating scheme would repeat bits using the same frequency band as the initial transmission. However, repeating in this way would increase the QP value of the injected waveform in the original frequency band, possibly violating the regulatory limit. For this reason, the repeating scheme proposed here uses a separate frequency band for each repeat. This preserves the low-data-rate property of each repeated-bit stream, allowing maximum transmitted power per repeated bit.

Fig. 3(a) illustrates the division of the f_β to $f_\beta + (R + 1)\ \Delta f$ kHz spectrum into $R + 1$ sub-spectra. The variable f_β indicates the lowest frequency employed for signaling. If the original symbol encodes a single bit, the maximum number of times a bit can be repeated is denoted as R. Thus, $R+1$ represents the number of sub-spectra utilized to transmit one bit. This strategy effectively leverages the QP regulations by maximizing the transmitted power per repeated bit because they occupy different sub-spectra. For instance, dividing the 150-210-kHz band (f_β is 150 kHz) into two 30 kHz (Δf) sub-spectra results in a maximum of $R = 1$ repeat. The 150-180-kHz sub-spectrum (150-180-kHz chirp signals) contains the original bit, while the 180-210-kHz sub-spectrum (180-210-kHz chirp signals) contains the first and only repeat. The original and repeated bit streams can equally maintain low data rates because they occupy different sub-spectra. In the 150-210-kHz band example, if a PLC modem receives an "up-chirp" from the 150-180-kHz sub-spectrum, it immediately repeats a 180-210-kHz "up-chirp". In this scheme, every modem in the network that successfully decodes the original bit simultaneously repeats it. This increases reliability because the proposed scheme offers PLC modems multiple chances to detect bits transmitted at higher power. Once again, employing different sub-spectra to repeat a bit limits data rates in each sub-spectrum and preserves

the CSS-QP-PLC benefits summarized in Section II-A. Other existing repeating schemes do not leverage the QP opportunity in this manner.

This section modifies the CSS-QP-PLC demodulation scheme proposed in [3] to account for repeating. Fig. 3(b) illustrates the strategy employed in the receiver (Rx) of the PLC modem to demodulate signals. Every sub-spectrum has its corresponding mixer, anti-aliasing low-pass filter (LPF), matched filters and threshold comparators. The modified receiver's matched filters are represented by

$$g_{ij}(t) = \int_0^T h_i(t-\tau) r_j(\tau) d\tau, \quad 0 < t < T. \tag{3}$$

Here $i = 0, 1$ corresponds to the received "down-chirp" and "up-chirp" signals respectively, $j = 1, \ldots, R+1$ indexes sub-spectra, and T denotes symbol duration. The impulse responses of the filters are given by

$$h_i(t) = x_i(T-t), \tag{4}$$

which is the same for all $R+1$ sub-spectra because the mixers shift the received signals $r_j(t)$ to the same baseband. The received signal $r_j(t)$ acquired from sub-spectrum j is

$$r_j(t) = \alpha_j(t) x_i(t) + n_j(t) \tag{5}$$

if a transmitted symbol is present, or

$$r_j(t) = n_j(t) \tag{6}$$

if absent, where $n_j(t)$ is band-limited noise and $\alpha_j(t)$ is the channel gain in sub-spectrum j.

A maximum *a posteriori* probability (MAP) rule determines the presence of $x_i(t)$ in $r_j(t)$. Assuming equal energy in $x_0(t)$ and $x_1(t)$, the received bit is "i" and determined to be transmitted through the j-th sub-spectrum if

$$\overline{g_{ij}(t)} - \overline{g_{\underline{i}j}(t)} > \frac{N_{0j}}{2} \ln\left(\frac{P_{\underline{i}}}{P_i}\right) \quad \forall \underline{i} \neq i \tag{7}$$

and

$$\overline{g_{ij}(t)} > \frac{1}{2} \int_0^T x_i^2(t) + \frac{N_{0j}}{2} \ln\left(\frac{P_2}{P_i}\right) \tag{8}$$

and

$$\overline{g_{ij}(t)} > \overline{g_{i\underline{j}}(t)} \quad \forall \underline{j} \neq j \tag{9}$$

are satisfied. In (7)–(9), $\overline{g_{ij}(t)}$ denotes the peak of $g_{ij}(t)$ while N_{0j} is the noise power. The parameter P_i is the *a priori* probability corresponding to (5) and P_2 is the *a priori* probability corresponding to (6). Afterwards, the PLC modem repeats the received bit "i" using the sub-spectrum with index $(j+1)$. Alternatively, if any condition in (7)–(9) remains unsatisfied, the received bit is invalid which is denoted as "2".

III. PROPOSED MEDIA ACCESS FRAMEWORK

The proposed PLC system presented in this work consists of device-modems and a coordinator-modem interconnected through an electrical power line network. A device-modem connects to a controllable electrical appliance such as a TCL. A coordinator-modem ensures the network operates efficiently. The proposed TDMA-based MAC protocol differs from typical TDMA protocols for many reasons. Firstly, the proposed protocol optimizes resource sharing among PLC modems for low-data-rate applications. Accordingly, TDMA-slot allocation primarily enables modems to leverage the QP opportunity and benefit from low-data-rate signaling. Reliability and coverage are prioritized over data throughput. Secondly, the proposed protocol seamlessly incorporates the distributed repeating scheme proposed in Section II-B. Finally, the proposed protocol framework was specifically developed for distributed load control. Underlying protocol parameters can be easily adapted to the specific application requirements.

Fig. 4(a) shows a snapshot of one communication period or session on the power line which lasts for Δt seconds. The proposed protocol divides a communication session into three time frames. The synchronization time frame is employed to synchronize all the modems in the network for the start of the TDMA time frame. The TDMA time frame is divided into time slots for modems to efficiently access the network and broadcast data. In the final time frame, all modems process the received data and perform application-specific tasks.

A. SYNCHRONIZATION

The coordinator-modem broadcasts a beacon message to initiate synchronization every communication session to limit and isolate possible synchronization errors. A beacon message is a known bit sequence that marks synchronization when correctly decoded. The devices retrieve and encode local information into a data packet after receiving the beacon message during the information-encoding period. Measured local temperature in the demand-leveling control of TCLs application exemplifies information encoded during this period. This period lasts for Δt_c seconds as shown in Fig. 4(a). The length of the synchronization time frame is given by

$$\Delta t_s = \frac{B}{c_s} + \Delta t_c \tag{10}$$

where B is the length of the beacon message in bits, c_s is the bit rate in the synchronization time frame in bps. Fig. 4(c) provides a clearer picture of the synchronization time frame. Synchronization occurs during the first $\Delta t_s = 10$ seconds in this example. The first eight pulses denote the eight-bit beacon message.

B. TDMA

During the TDMA time frame, modems share local information in a peer-to-peer manner for distributed control purposes.

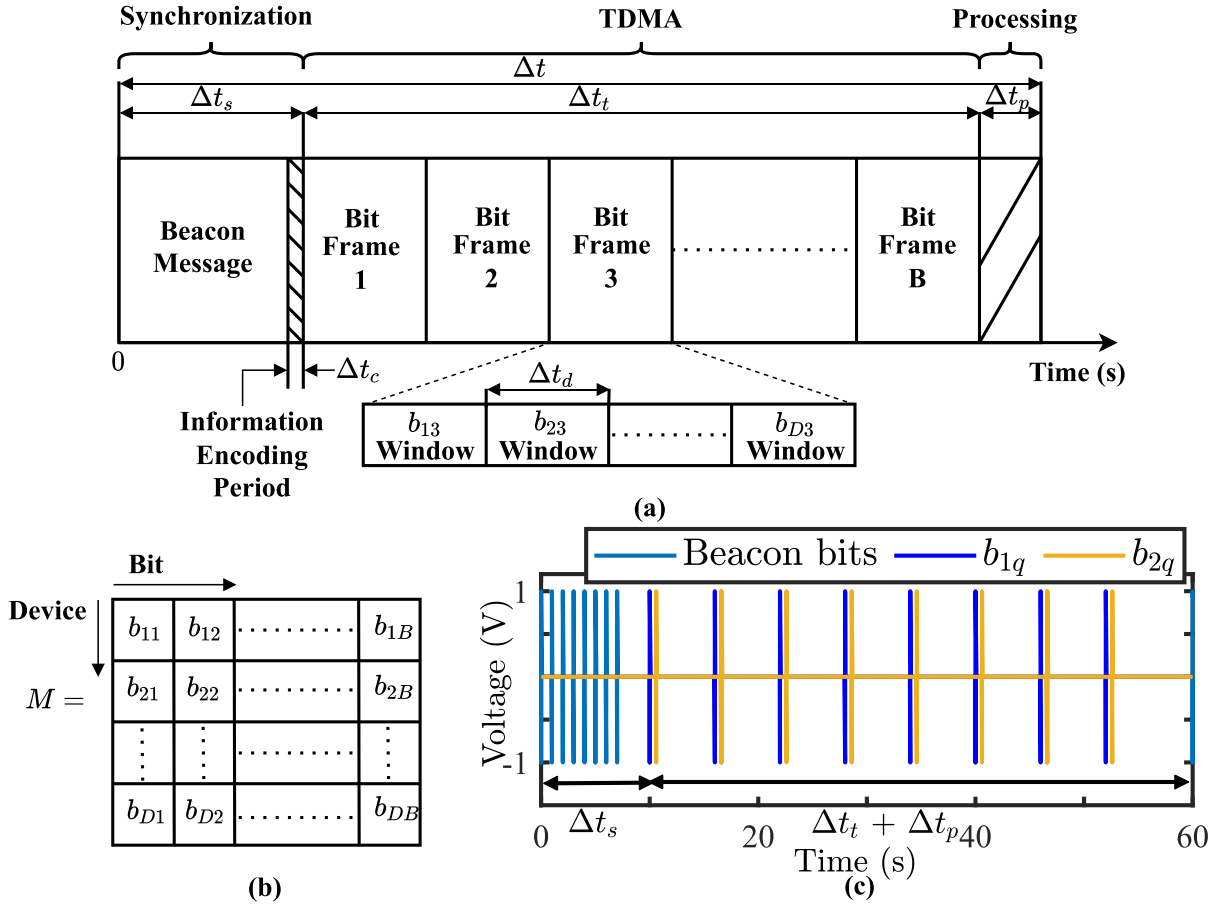

FIGURE 4. (a) The proposed TDMA-based network access protocol. (b) TDMA table. (c) Example TDMA-based network access protocol with $B = 8$ bits.

The table M in Fig. 4(b) is the network-wide TDMA table. The modems transmit bits b_{pq} during that TDMA time frame. The parameters $p = 1, \ldots, D$ and $q = 1, \ldots, B$ denote the modem identifier (ID) and bit index, respectively. Where D represents the maximum number of modems allowed in the network, including the coordinator-modem, and B is the length of a data packet in bits. Therefore, b_{pq} indicates the q-th bit in the p-th PLC modem's data packet. The first row in the TDMA table corresponds to the coordinator-modem ($p = 1$), whereas the other rows correspond to the device-modems based on their modem ID. Every modem in the network has its own local TDMA table. At the end of every TDMA time frame, in the absence of PLC errors, all modems should match their respective tables with the network-wide table.

Results published in [3] and summarized in Section II-A demonstrate that PLC coverage and reliability can be greatly improved by leveraging the QP regulations in low-data-rate PLC applications. Accordingly, the proposed access protocol preserves the low-data-rate signaling attribute by first dividing the TDMA time frame (Δt_t) into B bit frames instead of the typical D device frames. Afterwards, each bit frame is divided into D bit windows as illustrated in Fig. 4(a). As a result, the modems employ bit window b_{pq} to broadcast the q-th bit in the p-th PLC modem's data packet across the network. This includes the original b_{pq} bit and its R repeated copies. For instance, the modems transmit b_{p3} during bit frame 3 as illustrated in Fig. 4(a). Separating consecutive bits (b_{pq} and $b_{p(q+1)}$) in this manner limits data rate and maximizes transmitted power per bit. The length of the TDMA time frame is given by

$$\Delta t_t = B \Delta t_d D. \tag{11}$$

Section IV-D provides further justification for this particular TDMA time frame implementation.

Each modem keeps track of the current bit window by counting AC voltage line cycles from the start of the TDMA time frame. Every modem populates its local TDMA table depending on the current bit window. A modem transmits its bit when the current bit window corresponds to its row index in the TDMA table. Otherwise, the modem receives and repeats other modems' transmitted bits. Fig. 4(c) provides an

illustration of the TDMA time frame. This example includes two modems with eight bits per data packet. The TDMA time frame (between 10 and 55 seconds) demonstrates how both modems access their respective bit windows to broadcast information in each bit frame. Every pulse in Fig. 4(c) represents the original and repeated bits. The data-processing time frame begins after the TDMA time frame ends. In this time frame, each modem decodes the received data packets in their local TDMA table and performs application-specific tasks.

C. TDMA SLOT ASSIGNMENT

Immediately after joining the network, a new device-modem does not have a TDMA slot or modem ID (p). In this discussion, it is assumed that the number of available bit windows $D \times B$ have been optimized (and therefore, do not vary) for the specific distributed load control application. However, this work can be extended to account for dynamic number of modems D and packet length B [26]. Consequently, to get a TDMA slot, a new device-modem only decodes bits for Z TDMA time frames, indexed by $z = 1, \ldots, Z$, and populates its local TDMA table without broadcasting any data of its own. After observing the z-th TDMA time frame, the new device-modem identifies slot p_z as a candidate slot to claim, where p_z is one plus the index of the last occupied slot on the table. Mathematically,

$$p_z = \min \left\{ p \;\middle|\; \sum_{q=1}^{B} b_{aq} > B \text{ for all } a \geq p \right\}. \qquad (12)$$

In other words, a new device-modem starts at the bottom of the table and checks the condition in (12). This condition holds for slot p if slot p and all later slots are vacant. This is because the maximum sum of valid bits (“0”s or “1”s) is B. The rows corresponding to vacant slots will contain mostly “2”s, so their sum will likely exceed B. The process in (12) is repeated for Z TDMA time frames, at which point the device-modem claims slot $p^\star = \max\{p_1, \ldots, p_Z\}$. To improve robustness and reduce the probability of device-modems joining the network at the exact same instant selecting identical TDMA slots, each device-modem chooses their Z randomly. The new device-modem's ID/slot is stored in non-volatile memory to be used until it leaves the network.

IV. IMPLEMENTATION

The implementation of the proposed network access protocol depends on the application requirements and other constraints. This section highlights some of the implementation issues to consider when deploying the proposed protocol. In particular, Section IV-B validates the proposed repeating scheme and its impact on the implementation of the proposed access protocol. Additionally, Section IV-C describes approaches to tailoring the underlying system parameters to application-specific requirements.

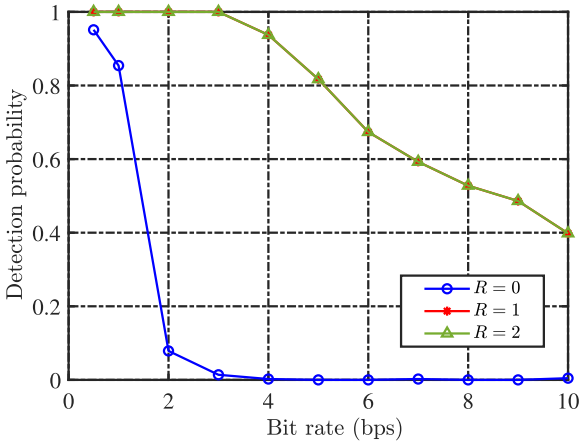

FIGURE 5. Effect of repeating on bit detection rate from the 13th floor to 24th floor of the test system employed in [3] and Section V-A.

A. SOFT FAILURE

The proposed protocol primarily fails when the coordinator-modem is unable to broadcast beacon messages. To account for this, the active device-modem occupying the earliest TDMA slot continuously monitors the presence of the coordinator-modem. This device-modem assumes the responsibility of synchronization if the network remains quiet for a pre-specified length of time. The coordinator-modem broadcasts a special “return” message via its TDMA slot after it returns and waits for the temporary coordinator-modem to correctly decode the “return” message. The coordinator-modem resumes synchronization after verifying network idleness for a pre-specified length of time.

B. REPEATING

Fig. 5 shows the performance of the proposed repeating scheme presented in Section II-B. This example employs the 150-180-kHz band to transmit the original bit. The 180-210-kHz and 210-240-kHz bands are utilized for the first and second repeated bits, respectively. The chirp signals represented by (1) and (2) are 2 ms long. The 24-floor apartment building presented in [3] and briefly discussed in Section V-A of this paper provides a case study. PLC modems are placed on the first, 13th, 14th and 24th floors. Fig. 5 demonstrates that repeating improves PLC reliability between the 13th and 24th floors. Without repeating, the probability of detecting a bit for rates between 0.5 and 10 bps is less than 100%. The detection rate increases when the modems on the first, 14th and 24th floors act as repeaters. Reliable PLC can be achieved at 3 bps when the original bit is repeated once. Fig. 5 also shows that repeating a second time does not increase bit detection rate. This can be seen from the near-exact matching of the red ($R = 1$) and green ($R = 2$) curves. While repeating the bit twice has no value in this case, this is not always true because power line networks widely vary in structure.

Certain design trade-offs have to be considered when implementing repeating in the proposed access protocol. The number of AC line cycles required to transmit a single bit or the length of a bit window,

$$\Delta t_d \geq R + 1, \tag{13}$$

increases with the number of repeats. The inequality sign in (13) ensures that the probability of receiving a repeated bit is high enough for the scheme to be beneficial. This is achieved by reducing the repeated-bit rate to leverage the QP regulations. As a result, repeating impacts the length of the communication period, Δt, or the number of modems that can access the network. Furthermore, the number of mixers, LPFs and matched filters increase with repeating as shown in Fig. 3. Also, more computation is required to simultaneously decode the bits in each sub-spectrum. This requires faster and more expensive processors. Consequently, trade-offs between size/cost/complexity and increased reliability due to repeating have to be considered in the implementation of the proposed network access protocol.

C. TIME CONSTRAINTS

In the proposed protocol, the communication period length Δt (shown in Fig. 4) is determined by the application requirements. For instance, applications such as the distributed control of TCLs set a time constraint on Δt for efficient performance. If Δt is large relative to the time constants of the TCLs, then temperature regulation will suffer. The communication delay due to the communication period length would lead to larger temperature deviations as Δt increases. Other applications such as the daily aggregation of automated meter readings do not require tight constraints on Δt. It can be as long as 24 hours in such applications. Consequently, the implementation of the proposed protocol depends on this constraint. This paper proposes a top-down implementation for time-constrained applications and a bottom-up approach for applications with loose or no constraints.

In the top-down approach, Δt is fixed and other parameters such as the maximum number of modems D are determined afterwards. For instance, the TCL control example in [5] with $\Delta t = 180$ seconds could have a TDMA time frame of $\Delta t_t = 160$ seconds. This would leave 20 seconds for synchronization and processing. In a 60-Hz system with $B = 8$ bits per data packet, all other parameters can be derived from

$$D\Delta t_d = \frac{\Delta t_t}{B} = 1200 \tag{14}$$

in AC line cycles. If the TCLs were located in the 24-floor apartment building presented in [3], then setting $\Delta t_d \geq 1/3$ seconds or 20 AC line cycles could provide reliable detection of the repeated bits. This can be seen from Fig. 6, which shows that a maximum of 3 bps data rate can be reliably achieved over all links in the network. For example, $\Delta t_d = 30$ AC line cycles would guarantee reliable PLC with

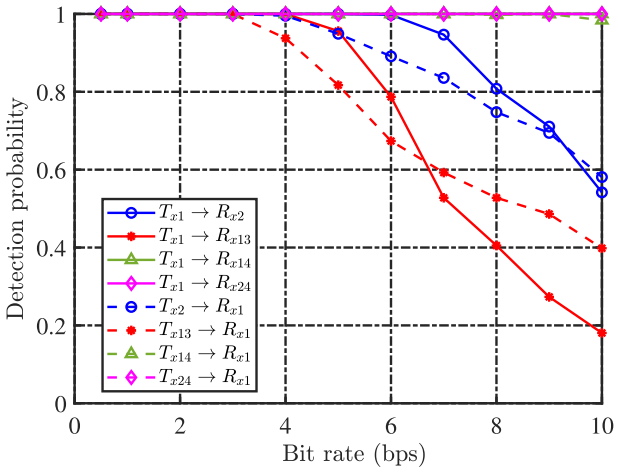

FIGURE 6. Detection probability vs. bit rate of key communication links in the test building utilized to select Δt_d and D given in Table 2. $T_{x1} \rightarrow R_{x2}$ corresponds to the transmitter on floor one and the receiver on floor two.

repeating. If additional prior knowledge of the PHY layer also shows that it requires $R = 1$, then the maximum number of TCLs in the network from (13) and (14) is 40.

In reality, the 24-floor apartment building has two electrical circuits as presented in [3]. Floors one and 14-24 are connected to one circuit while floors 2-13 are connected to the other circuit. Reliable PLC between the circuits can only be achieved at 3 bps while reliable PLC within each circuit can be achieved at slightly higher rates as shown in Fig. 6. Alternatively, two individual PLC networks can be created in this building for each electrical circuit. Fig. 6 shows that $\Delta t_d = 12$ AC line cycles can guarantee reliable PLC in each circuit for a 5 bps rate. Equations (13) and (14) show that 200 TCLs can be controlled in this building with the two-network implementation. The positive and negative zero crossings of the AC voltage line cycle can be assigned to the respective networks for the transmission of symbols. This eliminates symbol interference between the two networks.

The preceding discussion shows how parameters of the proposed protocol can be derived given Δt in the top-down approach. For applications with few or no time constraints, a bottom-up implementation is recommended. The designer should first select R, D and B before deriving Δt. For example, a daily meter aggregation application might have 500 power distribution feeders and a data packet of 100 Bytes. In this example, $\Delta t \approx 4$ hours if $R = 1$. In general, unconstrained applications can be made more reliable by increasing the number of repeats and channel coding through R and B, respectively.

D. TDMA TIME FRAME DIVISION

Section III-B proposed dividing the TDMA time frame into B bit frames before dividing each bit frame into D bit windows. An alternative (more conventional) approach is to divide the TDMA time frame into D device frames before dividing each device frame into B bit windows.

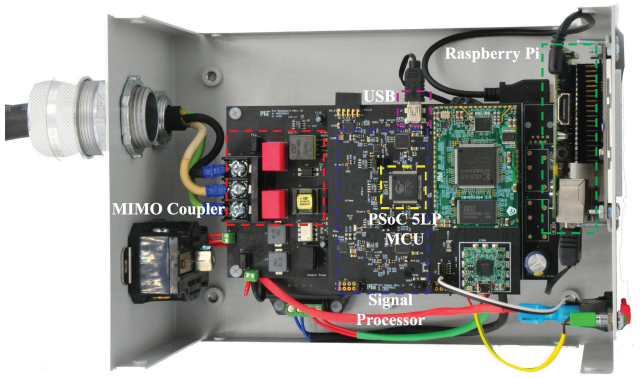

FIGURE 7. Top view of the hardware including PLC modem and Raspberry Pi employed to validate the effectiveness of the proposed network access protocol for distributed load control.

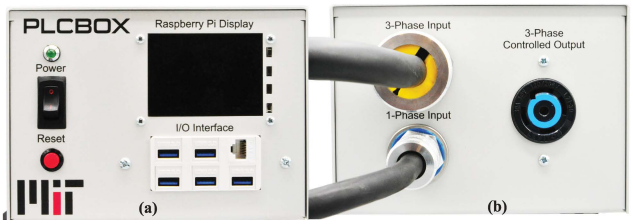

FIGURE 8. (a) Front view and (b) back view of the hardware device employed to validate the performance of the proposed network access protocol.

This means that modem p broadcasts all its B bits before modem $p+1$ transmits at all.

In a TCL control example with $\Delta t_t = 160$ seconds, $\Delta t_d = 30$ AC line cycles and $D = 40$ modems, under the proposed approach, each modem communicates one bit every 1200 AC line cycles. In the alternative approach, however, the achievable data rate per modem derived from (11) and (14) is

$$\frac{1}{\Delta t_d} = \frac{40}{1200}, \tag{15}$$

which corresponds to one bit every 30 AC line cycles. In CSS-QP-PLC, the proposed approach is preferable due to its lower data rate per modem. The QP regulations allow the transmitted power per bit to increase as the data rate decreases [3]. This increases the probability of detecting a bit when employing the proposed approach.

V. DEMONSTRATION

Ultimately, most communication systems, including the proposed PLC system, are designed to meet and provide application-specific objectives and services, respectively. As a result, this section presents a field demonstration of distributed TCL control. This paper utilizes this demonstration to validate the efficacy of the proposed repeating and access protocol schemes for distributed load control.

A. EXPERIMENTAL SETUP

The experimental demonstration consists of multiple hardware devices and a test environment. A hardware device is a PLC modem and computing platform, e.g. a Raspberry Pi, shown in Fig. 7. The PLC modem couples the chirp signal between the high-voltage power line and low-voltage signal processing section with a multiple-input and multiple-output (MIMO) circuit. The MIMO circuit shown in Fig. 7 consists of transformers, solid-state relays and capacitors. A detailed circuit diagram of the MIMO coupler is provided in [3]. The signal processing section employs two Texas Instruments AFE032 analog front-ends (AFEs) for signal conditioning and a Cypress PSoC 5LP microcontroller (MCU) for discrete-time signal processing. The AFEs are programmable devices designed to operate in the NB-PLC frequency band. They consist of configurable filters, power amplifiers and programmable gain amplifiers. The MCU configures the AFEs through a serial peripheral interface. The PHY layer which includes the chirp modulator in the transmitter; mixers, matched filters and threshold comparators in the receiver are implemented on the PSoC MCU. The proposed network access protocol is also implemented on the MCU. A more detailed description of the PLC modem circuitry can be found in [3]. The device can either operate in control or emulation mode. In control mode, the device directly controls a single-phase or three-phase electrical load (e.g., a TCL) through on-board relays. The load connects to the device through the "3-Phase Controlled Output" port shown in Fig. 8(b). The device does not control a real electrical load in emulation mode. Instead, a Raspberry Pi simulates the dynamics of the electrical load and its environment (e.g., a TCL and its thermal circuit) and exchanges information with the MCU through a universal serial bus (USB). The results presented in this section are based on operating the devices in emulation mode in a building. The experiments reported here were conducted in eight-hour intervals and replicated daily for three weeks in September, 2021.

The hardware devices create a PLC network in a 24-floor high-rise apartment building located on the campus of the Massachusetts Institute of Technology shown in Fig. 9. In a real-world application, a PLC device-modem would control a TCL operating in this building to meet demand-response obligations. This apartment building has two electrical circuits that are connected at the main distribution panel in the basement. The electrical circuit diagram and more details of this building are provided in [3]. Floors 2-13 are connected to one circuit, while floors one and 14-24 are connected to the other circuit as previously mentioned in Section IV-C. Signals experience deleterious attenuation as high as 80 dB in this building [3]. This is because communication signals travel longer distances and through more circuit breakers when crossing from one circuit to the other. The CSS-QP-PLC technique proposed in [3], the repeating scheme and network access protocol proposed in this paper can be employed to create a reliable PLC network despite the challenging attenuation profiles in this building.

FIGURE 9. Field demonstrations are set in a 24-floor high-rise apartment building on the campus of the Massachusetts Institute of Technology.

Relative to many smart-grid PLC field experiments in the existing literature [27]–[29], the experimental environment considered in this work is comparatively challenging. For example, in [27], air conditioners are controlled to shave peak demand using PLC links with signal-to-noise ratio between 10 to 24 dB. By contrast, the PLC links in the test building considered here experience signal-to-noise ratio as low as 3 to 4 dB. Also, because the test building has 24 floors with over 400 rooms, the large number of electrical loads and long runs of wires drastically increase PLC channel attenuation (as high as 80 dB) and noise [3]. In similar works with field demonstrations, experiments are typically performed in laboratory environments [28] or two-storey three-bedroom residential houses with less challenging PLC conditions [29].

B. DISTRIBUTED CONTROL OF TCLs

TCLs can reduce their peak power demand while regulating temperature through a variety of control schemes [5]. This paper applies the distributed control of TCLs framework presented in [5] to validate the performance of the proposed network access protocol. It should be noted that the purpose of this study is only focused on the applicability of the proposed protocol to a real-world smart grid application, not necessarily on the application itself.

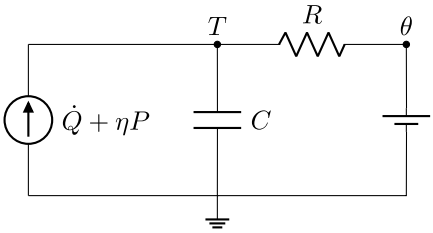

FIGURE 10. A 1R1C thermal circuit. The ambient temperature θ and thermal power $\dot{Q}+\eta P$ play the roles of voltage and current sources, respectively.

1) PROBLEM STATEMENT

The distributed control of TCLs framework involves a set $\mathcal{L} = \{1, \ldots, L\}$ of TCLs and a discrete time span $\mathcal{K} = \{1, \ldots, K\}$. At each time $k \in \mathcal{K}$, each TCL $\ell \in \mathcal{L}$ observes its local temperature $T_\ell(k)$ in °C and receives additional information through the power line from the other TCLs. Each TCL ℓ then decides its control input

$$u_\ell(k) \in \{0, 1\} \tag{16}$$

with 0 meaning "OFF" and 1 meaning "ON".

This paper employs the first-order thermal circuit shown in Fig. 10 to model the thermal environment with the TCL in heating mode. The input signals are the electric power P in kW used by the TCL, the surrounding temperature θ in °C, and the thermal power $\dot{Q}$ in kW from external sources. The parameters are the resistance R in °C/kW, the capacitance C in kWh/°C, and coefficient of performance η. Assuming a zero-order hold on the input signals, the discrete-time dynamics are

$$T(k+1) = aT(k)+(1-a)[\theta(k)+R(\dot{Q}(k)+\eta P(k))] \tag{17}$$

where $a = \exp(-\Delta t/(RC))$ and Δt in hours is the application and communication period. The Raspberry Pi simulates the above dynamics of the thermal circuit to emulate a TCL and its thermal load. The load temperature should satisfy

$$T^{\text{set}}(k) - \epsilon \le T(k) \le T^{\text{set}}(k) + \epsilon \tag{18}$$

where $T^{\text{set}}(k)$ in °C is a user-specified setpoint and ϵ in °C is the halfwidth of a band of acceptable temperatures. A brief discussion of the TCL modeling framework has only been provided here, a more detailed derivation can be found in [5].

2) DISTRIBUTED CONTROL

The distributed control algorithm originally proposed in [5] and presented here limits the peak demand of the TCLs

$$\max_{k\in\mathcal{K}} \sum_{\ell\in\mathcal{L}} P_\ell(k) = \max_{k\in\mathcal{K}} \sum_{\ell\in\mathcal{L}} u_\ell(k)\overline{P}_\ell \le P^{\text{cap}}. \tag{19}$$

Here, $\overline{P}_\ell$ is the TCL's capacity and P^{cap} represents a given aggregate TCL power demand cap typically set based on historical data and broadcast to the TCLs by the system coordinator-modem. The TCLs should also satisfy the ON/OFF constraint in (16) and the temperature constraint in (18).

This paper employs the "on-time" priority control method presented in [5] due to its low communication requirements. Each TCL determines its "current" state $v_\ell(k)$ during the information encoding period and broadcasts it during the TDMA time frame. Where,

$$v_\ell(k) = \begin{cases} 0 & \text{if } u_\ell(k) = 0 \\ & \text{and (18) is satisfied} \\ 1 & \text{if } u_\ell(k) = 1 \\ 2 & \text{if } u_\ell(k) = 0 \\ & \text{and (18) is not satisfied.} \end{cases} \tag{20}$$

Each TCL locally computes a priority score $\lambda_\ell(k)$ for every TCL in the network during the processing time frame. This score is equal to $v_\ell(k)$. A tie among multiple TCLs, when $v_\ell(k) = 1$ or $v_\ell(k) = 2$, is broken through "on-times". The TCL with the lower "on-time" when $v_\ell(k) = 1$ for multiple TCLs has a higher priority, while the opposite is true when $v_\ell(k) = 2$. The number of consecutive periods the "current state" v_ℓ was equal to 1 or 2 provides an estimate for the "on-time" of TCL ℓ. Afterwards, each TCL ranks every TCL, including itself, based on their priority scores $\lambda_\ell(k)$. Each TCL goes through the priority list in ascending order and removes the TCLs with the lowest scores until the constraint in (19) is satisfied. It is assumed that every TCL broadcasts its size $\overline{P}_\ell$ once after joining the network. Finally, each TCL locally determines its control input for the next time step $u_\ell(k+1)$ depending on its presence - 1 - or absence - 0 - in the pruned priority list.

3) COMMUNICATION

The TCLs utilize the proposed network access protocol to broadcast their states $v_\ell(k)$. Typical time constants of thermal circuits given in Table 1 [5] constraints the implementation of the access protocol. The length of a communication period Δt results from the average time constants and outdoor temperatures of the thermal circuits in the building. The dynamics of the circuit in Fig. 10 and the worst-case acceptable temperature deviation from $T^{\text{set}} - \epsilon$ when $v_\ell(k) = 2$ provide an estimate for Δt. Each TCL transmits a data packet with eight bits every TDMA time frame. The coordinator-modem encodes P^{cap} as a percentage of the total TCL capacity in the network with a four-bit payload. A four-bit payload also encodes the TCL state $v_\ell(k)$. The remaining four bits are preambles and sum checkers. The network protocol parameters given in Table 2 have already been derived in Section IV-C. This paper only employs four TCLs and one coordinator-modem to validate the performance of the proposed protocol because of limited resources. However, Table 2 shows that 195 additional TCLs can join the networks created in the apartment building.

In this study, the 150-180-kHz and 180-210-kHz spectral channels are used to transmit original and repeated bits, respectively. Therefore, 150-180-kHz and 180-210-kHz linear chirp signals, defined in (1) and (2), modulate the transmitted bits. The chirp signals have a 2 ms duration and are shown in Fig. 2. Fig. 3(b) illustrates the procedure for demodulating received signals. The mixer corresponding to the 150-180-kHz channel has a 190-kHz local-oscillator frequency, whereas, the mixer corresponding to the 180-210-kHz channel has a 220-kHz local-oscillator frequency. Therefore, the received baseband signals occupy the 10-40-kHz spectrum. These baseband signals are sampled at 500 ksps, with the anti-aliasing LPFs cut-off frequency at 45 kHz. The impulse responses of the matched filters are represented by (4). Due to the effect of mixing the 150-180-kHz and 180-210-kHz chirp signals to the 10-40-kHz baseband, $x_0(t)$ and $x_1(t)$ in (4) now correspond to a 10-40-kHz "up-chirp" and "down-chrip" signals, respectively. For threshold comparison, the MAP rule detector in (7) assumes $P_0 = P_1$, therefore, the right-hand side of (7) reduces to zero. Finally, the right-hand side of (8) is determined from the measured noise at the receiver.

TABLE 1. Application Parameters.

Parameter	Value
Number of TCLs, L	4
Time step, Δt (hours)	3/60
Thermal resistance, R (°C/kW)	[5,5.2,6,5.5]
Thermal capacitance, C(kWh/°C)	[1.5,2,1.75,2.5]
Coefficient of performance, η	[3.5,3.5,3.5,3.5]
Deadband halfwidth, ϵ (°C)	[0.5,0.5,0.5,0.5]
Outdoor temperature, θ (°C)	[10,9.8,9.2,9]
External thermal power, $\dot{Q}$ (kW)	[0.25,0.35,0.45,0.4]

TABLE 2. Communication Parameters.

Parameter	Value
Synchronization time, Δt_s (s)	9
Processing time, Δt_p (s)	11
Maximum number of modems, D	200
Packet length, B (Byte)	1
Number of bit repeats, R	1

4) RESULTS AND DISCUSSION

This section presents one eight-hour experiment in the test environment to validate the performance of the proposed access protocol. The coordinator-modem (24th floor) and TCLs (24th, 21st, 18th and 14th floors) are connected to the same electrical circuit of the apartment building. The results presented here are similar when the modems are all connected to the other circuit of the 24-floor high-rise apartment building. The user-specified setpoint T^{set} and capacity $\overline{P}_\ell$ for the TCLs are 22.2 °C and 3 kW, respectively. Fig. 11(a) and (b) show the temperatures and aggregate power demanded by the TCLs for the "on-time" priority-based distributed control case, respectively. The coordinator-modem continuously broadcasts $P^{\text{cap}} = 3$ kW during the first four hours of the simulation. Fig. 11(a) and (b) show that the TCLs are able to adequately regulate peak power demand and temperatures. The coordinator-modem increases $\overline{P}_\ell$ to 6 kW between the fourth and sixth hour before decreasing it to 3 kW for the final two hours. Again, the power and

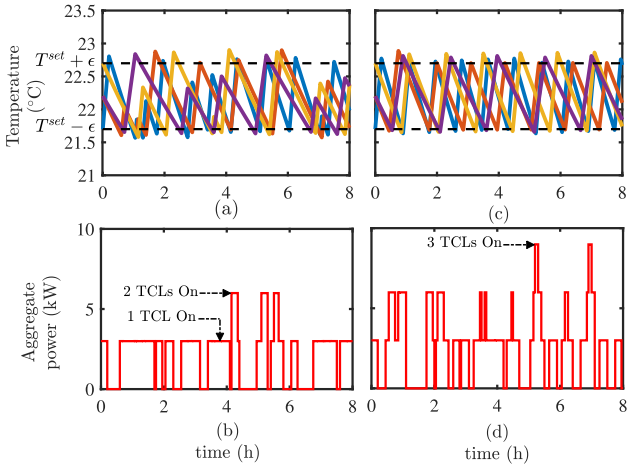

FIGURE 11. Control of TCLs with $\Delta t = 3$ minutes. (a) Thermal load temperatures with distributed control. (b) Aggregate TCL power demand with distributed control. (c) Thermal load temperatures with "bang-bang" control. (d) Aggregate TCL power demand with "bang-bang" control.

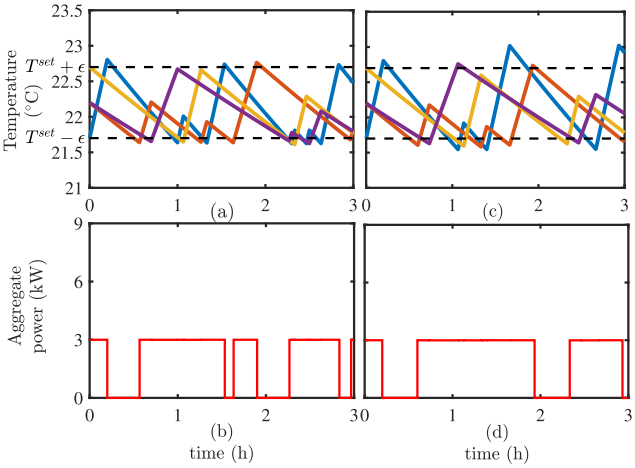

FIGURE 12. Distributed control of TCLs. (a) Thermal load temperatures with $\Delta t = 2$ minutes. (b) Aggregate TCL power demand with $\Delta t = 2$ minutes. (c) Thermal load temperatures with $\Delta t = 4$ minutes. (d) Aggregate TCL power demand with $\Delta t = 4$ minutes.

temperature constraints are adequately met during these periods. Fig. 11(a) and (b) show that the control algorithm implemented with the proposed protocol sufficiently limits peak power demand while adequately regulating temperatures. Comparing Fig. 11(a) and (b) with Fig. 11(c) and (d) emphasizes the benefit of the distributed communication and control algorithms. Fig. 11(c) and (d) show the impact of controlling the TCLs in the conventional "bang-bang" control mode. The aggregate power consumed by the TCLs fluctuates randomly and gets as high as 9 kW without employing the distributed communication and control algorithms.

Furthermore, it can be observed by comparing Fig. 11(a) with Fig. 11(c) that "bang-bang" control regulates the temperatures better than the distributed control strategy. This is obvious from differences in temperature deviations below the allowable temperature band $T^{\text{set}} - \epsilon$. These deviations result from communication delays in broadcasting $v_\ell(k)$ due to Δt. Fig. 12(a) shows that decreasing Δt to two minutes reduces these deviations. However, the number of devices that can access the network decreases if all other parameters in Table 2 remain unchanged. The number of devices can alternatively be increased by changing Δt to four minutes. However, Fig. 12(c) shows that this will cause further deviations below $T^{\text{set}} - \epsilon$. This might be worth the benefit of having more devices join the network in certain situations. Nevertheless, Fig. 12(c) and (d) show adequate regulation of peak power demand irrespective of the value of Δt. Finally, the temperature deviations above $T^{\text{set}} + \epsilon$ in Fig. 11 and 12 are an artefact of the time-domain simulation solver. In reality, the TCL's controller turns off the TCL immediately the measured temperature from the sensor reaches $T^{\text{set}} + \epsilon$. This paper only employed the distributed control of TCLs to highlight the efficacy of the proposed network access protocol. The proposed protocol is very flexible and can be applied to other low-data-rate control and sensing applications.

VI. CONCLUSION

This paper carefully has tailored a novel power-line communication system to smart grid applications, where low data rates are acceptable but reliability must be high. This paper has experimentally validated the full communication stack, including an application layer that implements a recently-developed method for distributed load control. These experiments build confidence in the suitability of both the communication system and the load-control method for non-intrusive demand-response schemes. Interesting directions for future work include dynamically updating the TDMA table structure as devices join or leave the network, adaptively tuning receiver parameters to unfamiliar environments or time-varying channel conditions, and experimentally evaluating the communication system for other applications, such as frequency regulation or voltage support.

REFERENCES

[1] S. C. Shabshab, P. A. Lindahl, J. K. Nowocin, and S. B. Leeb, "Voltage waveform transient identification for autonomous load coordination," *IEEE Access*, vol. 7, pp. 123128–123137, 2019.
[2] W.-T. Li, C. Yuen, N. U. Hassan, W. Tushar, C.-K. Wen, K. L. Wood, K. Hu, and X. Liu, "Demand response management for residential smart grid: From theory to practice," *IEEE Access*, vol. 3, pp. 2431–2440, 2015.
[3] A. Aderibole, E. K. Saathoff, K. Kircher, S. Leeb, and L. K. Norford, "Power line communication for low-bandwidth control and sensing," *IEEE Trans. Power Del.*, early access, Aug. 20, 2021, doi: 10.1109/TPWRD.2021.3106585.
[4] S. C. Shabshab, P. A. Lindahl, S. B. Leeb, and J. K. Nowocin, "Autonomous demand smoothing for efficiency improvements on military forward operating bases," *IEEE Trans. Power Del.*, vol. 35, no. 5, pp. 2243–2251, Oct. 2020.
[5] K. Kircher, A. Aderibole, L. K. Norford, and S. Leeb, "Distributed peak shaving for small aggregations of cyclic loads," *IEEE Trans. Power Del.*, early access, Feb. 8, 2022, doi: 10.1109/TPWRD.2022.3149446.
[6] F. Rahimi and A. Ipakchi, "Overview of demand response under the smart grid and market paradigms," in *Proc. Innov. Smart Grid Technol. (ISGT)*, Jan. 2010, pp. 1–7.
[7] L. Jian, H. Xue, G. Xu, X. Zhu, D. Zhao, and Z. Y. Shao, "Regulated charging of plug-in hybrid electric vehicles for minimizing load variance in household smart microgrid," *IEEE Trans. Ind. Electron.*, vol. 60, no. 8, pp. 3218–3226, Aug. 2013.

[8] S. Barker, A. Mishra, D. Irwin, P. Shenoy, and J. Albrecht, "SmartCap: Flattening peak electricity demand in smart Homes," in *Proc. IEEE Int. Conf. Pervasive Comput. Commun.*, Mar. 2012, pp. 67–75.
[9] D. P. F. Moller and H. Vakilzadian, "Ubiquitous networks: Power line communication and Internet of Things in smart home environments," in *Proc. IEEE Int. Conf. Electro/Inf. Technol.*, Jun. 2014, pp. 596–601.
[10] Y. Chen and J. K. Hwang, "A reliable energy information system for promoting voluntary energy conservation benefits," *IEEE Trans. Power Del.*, vol. 21, no. 1, pp. 102–107, Jan. 2006.
[11] J. Matanza, S. Alexandres, and C. Rodríguez-Morcillo, "Advanced metering infrastructure performance using European low-voltage power line communication networks," *IET Commun.*, vol. 8, no. 7, pp. 1041–1047, May 2014.
[12] R. M. de Oliveira, A. B. Vieira, H. A. Latchman, and M. V. Ribeiro, "Medium access control protocols for power line communication: A survey," *IEEE Commun. Surveys Tuts.*, vol. 21, no. 1, pp. 920–939, 1st Quart., 2019.
[13] L. Di Bert, S. D'Alessandro, and A. M. Tonello, "MAC enhancements for G3-PLC home networks," in *Proc. IEEE 17th Int. Symp. Power Line Commun. Appl.*, Mar. 2013, pp. 155–160.
[14] A. M. Sarafi, A. C. Voulkidis, and P. G. Cottis, "Optimal TDMA scheduling in tree-based power-line communication networks," *IEEE Trans. Power Del.*, vol. 29, no. 5, pp. 2189–2196, Oct. 2014.
[15] S. Choe, J. Yoo, and Y. Louet, "Cluster-based MAC and resource management for quasi-stationary broadband power line communication networks," in *Proc. IEEE 17th Int. Symp. Power Line Commun. Appl.*, Mar. 2013, pp. 64–68.
[16] A. M. Tonello, J. A. Cortes, and S. D'Alessandro, "Optimal time slot design in an OFDM-TDMA system over power-line time-variant channels," in *Proc. IEEE Int. Symp. Power Line Commun. Appl.*, Mar. 2009, pp. 41–46.
[17] B. Sivaneasan, P. L. So, and E. Gunawan, "A hybrid contention-polling protocol for PLC-based AMR systems," in *Proc. Conf. (IPEC)*, Oct. 2010, pp. 1152–1157.
[18] A. Zaballos, G. J. Ravera, A. Vallejo, and J. M. Selga, "Simulation and modeling of the coexistence of polling and contention in PLC based AMR systems," in *Proc. IEEE Int. Symp. Power Line Commun. Appl.*, Mar. 2007, pp. 110–115.
[19] Y. Huo, G. Prasad, L. Lampe, and V. C. M. Leung, "Efficient access control for broadband power line communications in home area networks," *IEEE Trans. Commun.*, vol. 66, no. 4, pp. 1649–1660, Apr. 2018.
[20] Y. Ben-Yehezkel, R. Gazit, and A. Haidine, "Performance evaluation of medium access control mechanisms in high-speed narrowband PLC for smart grid applications," in *Proc. IEEE Int. Symp. Power Line Commun. Appl.*, Mar. 2012, pp. 94–101.
[21] K. Ashrafuzzaman and A. O. Fapojuwo, "Analytic modeling of CSMA/CA based differentiated access control with mixed priorities for smart utility networks," in *Proc. IEEE Int. Conf. Commun. (ICC)*, Jun. 2014, pp. 3694–3699.
[22] M. H. L. Chan and R. W. Donaldson, "Attenuation of communication signals on residential and commercial intrabuilding power-distribution circuits," *IEEE Trans. Electromagn. Compat.*, vol. EMC-28, no. 4, pp. 220–230, Nov. 1986.
[23] D. Radford, "Spread spectrum data leap through AC power wiring," *IEEE Spectr.*, vol. 33, no. 11, pp. 48–53, Nov. 1996.
[24] *Specification for Radio Disturbance and Immunity Measuring Apparatus and Methods—Part 1-1: Radio Disturbance and Immunity Measuring Apparatus-Measuring Apparatus*, document CISPR, 16-1-1, 2015.
[25] M. Girotto and A. M. Tonello, "EMC regulations and spectral constraints for multicarrier modulation in PLC," *IEEE Access*, vol. 5, pp. 4954–4966, 2017.
[26] I. Jabandzic, S. Giannoulis, R. Mennes, F. A. P. D. Figueiredo, M. Claeys, and I. Moerman, "A dynamic distributed multi-channel TDMA slot management protocol for ad hoc networks," *IEEE Access*, vol. 9, pp. 61864–61886, 2021.
[27] S.-C. Hsieh, T.-T. Ku, C.-S. Chen, C.-H. Lin, and J.-C. Tsai, "Broadcasting control of intelligent air conditioners using power-line-carrier technology," *IEEE Trans. Ind. Appl.*, vol. 51, no. 2, pp. 1890–1896, Mar./Apr. 2015.
[28] D. S. Kim, S. Y. Lee, K. Y. Wang, J. C. Choi, and D. J. Chung, "A power line communication modem based on adaptively received signal detection for networked home appliances," *IEEE Trans. Consum. Electron.*, vol. 53, no. 3, pp. 864–870, Aug. 2007.
[29] S. Barker, D. Irwin, and P. Shenoy, "Pervasive energy monitoring and control through low-bandwidth power line communication," *IEEE Internet Things J.*, vol. 4, no. 5, pp. 1349–1359, Oct. 2017.

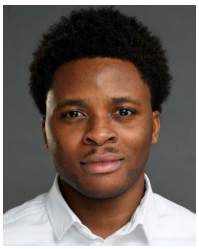

ADEDAYO O. ADERIBOLE received the B.Sc. degree in electronic/electrical engineering from Obafemi Awolowo University, Ife, Nigeria, in 2013, and the M.Sc. degree in electrical power engineering from the Masdar Institute, Khalifa University of Science and Technology, Abu Dhabi, United Arab Emirates, in 2017. He is currently pursuing the Ph.D. degree in electrical engineering and computer science with the Massachusetts Institute of Technology, Cambridge, MA, USA. His research interests include communication theory, signal processing, and power system modeling and control.

KEVIN J. KIRCHER (Member, IEEE) received the Ph.D. degree in mechanical engineering from Cornell University, in 2019. He is currently a Postdoctoral Researcher in electrical engineering and computer science at the Massachusetts Institute of Technology. His research interests include learning, optimization, and control methods to smart buildings, focusing on their interaction with the electrical grid.

STEVEN B. LEEB (Fellow, IEEE) received the Ph.D. degree from the Massachusetts Institute of Technology, in 1993. He was a Commissioned Officer at USAF Reserves. He has been a member of the Department of Electrical Engineering and Computer Science, Massachusetts Institute of Technology (MIT), since 1993. He also holds a joint appointment at the Department of Mechanical Engineering, MIT. He is the author or coauthor of over 200 publications and 20 U.S. patents in the fields of electromechanics and power electronics.

LESLIE K. NORFORD received the Ph.D. degree in mechanical and aerospace engineering from Princeton University, in 1984, after five years of active duty as a Nuclear Power Officer at the U.S. Navy. He has been a member of the Department of Architecture, Massachusetts Institute of Technology, since 1988. His research interests include design, operation, and fault detection of space conditioning systems for low-carbon buildings and interactions of buildings with the electrical grid and with urban environments.